J Mater Sci (2012) 47:1077–1084
DOI 10.1007/s10853-011-5898-5

Elaboration and mechanical characterization of multi-phase alumina-based ultra-fine composites

Paola Palmero · Antonella Sola · Valentina Naglieri · Devis Bellucci · Mariangela Lombardi · Valeria Cannillo

Received: 3 July 2011 / Accepted: 23 August 2011 / Published online: 7 September 2011

Abstract Al_2O_3-10 vol.% YAG and Al_2O_3-10 vol.% ZrO_2 bi-phase composites as well as Al_2O_3-5 vol.% YAG-5 vol.% ZrO_2 tri-phase composite were developed by controlled surface modification of an alumina powder with inorganic precursors of the second phases. Green bodies were produced by dry pressing and slip casting and then sintered at 1500 °C. In particular, slip casting led to fully dense, defect-free, and highly homogenous samples, made of a fine dispersion of the second phases into the micronic alumina matrix, as observed by SEM. The mechanical characterization proved the predominant role of the final density on the Vickers hardness, while the elastic modulus was affected by the volume fraction of the constituent phases, in fairly good agreement with the rule of mixture prediction. The fracture toughness values of the bi- and tri-phase materials were similar, and their crack paths revealed the importance of the thermal residual stresses at the matrix-reinforcement interfaces, promoting intergranular propagations.

Introduction

In many industrial applications, ceramic components are required to work in extremely harsh conditions, particularly at very high temperatures for long times, and such requirements can be met by the exploitation of micro/nanocomposites. For their design, a suitable choice of the matrix and second phases must be performed; moreover, the number, volume fraction, size, and morphology of the reinforcing phases must be properly set as well [1]. As regards the alumina-based composites, the Alumina–$Y_3Al_5O_{12}$ (YAG) system presents interesting properties at room and, particularly, at high temperature [2–7], mainly thanks to the excellent creep resistance of the YAG phase [8]. Alumina–ZrO_2 composites have been also widely investigated [9–12]; in this system, alumina provides high strength whereas tetragonal zirconia exerts a toughening effect thanks to its controlled transformation into the monoclinic phase [9, 13]. Indeed, if fully stabilized in cubic form, zirconia becomes extremely interesting for high-temperature applications: in fact, cubic zirconia (c-ZrO_2) is currently used as a solid electrolyte in solid oxide fuel cells (thanks to its excellent stability and high oxygen ionic conductivity over a wide range of temperatures and oxygen partial pressures [14]) and even applied in thermal barrier coatings because of its low thermal conductivity and good erosion resistance [14]. Some multi-phase micro/nanocomposite oxide ceramics have been recently developed [15–19], with the aim of further increasing the mechanical properties through a more strict control of the microstructural features. For instance, Kim et al. [18] elaborated a 33 vol.%Alumina-33 vol.%YAG-33 vol.%Zirconia composite, with the aim of producing materials with high strength retention even after prolonged high temperature annealing, while Oelgardt et al. [19] produced and tested an ultra-fine composite in the same system, with an eutectic composition, with the aim of comparing its basic mechanical properties to those presented by materials obtained by directional solidification from eutectic melts.

P. Palmero (✉) · V. Naglieri · M. Lombardi
Dipartimento di Ingegneria Chimica E Scienza Dei Materiali, Politecnico di Torino, INSTM, R.U. PoliTO, LINCE Lab, Corso Duca degli Abruzzi 24, 10129 Turin, Italy
e-mail: paola.palmero@polito.it

A. Sola · D. Bellucci · V. Cannillo
Dipartimento di Ingegneria Dei Materiali E Dell'Ambiente, Università di Modena E Reggio Emilia, INSTM, R.U. UniMORE, LINCE Lab, Via Vignolese 905, 41125 Modena, Italy

In this article, two biphasic composites, namely Al_2O_3–10 vol.%YAG (AY) and Al_2O_3–10 vol.%. Fully Stabilized Zirconia (AZ), and a triphasic material, Al_2O_3–5 vol.%YAG-5 vol.%. Fully Stabilized Zirconia (AZY), were developed. With respect to the previous literature, this study intends to compare the effect of a double-phase reinforcement versus a single-phase one in composites having the same total amount of the second phases. With this purpose, the three fully dense composites were submitted to a basic mechanical characterization and the results were discussed on the basis of their different microstructural features.

Experimental

Composite powders elaboration

A well-dispersed α-alumina (TM-DAR TAIMICRON, supplied by Taimei Chemical Co., Japan [20]) slurry was employed to develop the composite powders, following a procedure already described in the literature [21, 22]. Briefly, aqueous solutions of $YCl_3 \cdot 6H_2O$ (Aldrich, 99.99% purity) and $ZrCl_4$ (Fluka, >98% purity) were prepared and dropwise added to the α-alumina dispersed suspension to prepare Alumina–10 vol%YAG (here labeled as AY), Alumina–10 vol.%Y-FSZ (AZ), and Alumina–5 vol%YAG-5 vol% Y-FSZ (AZY) composite powders. In the latter material, the yttrium salt concentration was determined by considering its double role: in fact, upon thermal treatment, it reacts with alumina to yield YAG and also provides full stabilization of cubic zirconia.

According to a previous study [23], AZ was pre-treated at 600 °C for 1 h at the heating rate of 10 °C/min. Conversely, AY was submitted to some calcination treatments in the 1050–1200 °C temperature range, by both applying "conventional" and "fast" treatments. The former was carried out heating the samples at 10 °C/min, the latter was performed by instantaneously plunging the powder into a vertical furnace kept at the fixed temperature for a short time (5 min). This last procedure was set-up for limiting the second phase crystallites growth, as demonstrated in a previous study [24]. On the basis of XRD analyses (Philips PW1710) carried out on the differently calcined AZ and AY, the pre-treatment conditions of AZY were finally set-up.

Forming, sintering and microstructural characterization

Aqueous suspensions of pre-treated powders (with solid loads of 65 wt%) were prepared and dispersed by ball-milling (powder/α-Al_2O_3 spheres weight ratio of 1/5) for 48–96 h.

Green bodies were obtained by slip casting the dispersed slurries into porous moulds, followed by a drying step in a humidity-controlled chamber for about 1 week. For comparison, green bars of dispersed AY, AZ, and AZY powders were also prepared by uniaxial pressing at 300 MPa. The green densities were evaluated by mass and geometric measurements.

Slip cast as well as pressed green bodies were sintered up to 1500 °C for 3 h. The final density of the composites was determined by Archimedes's method and referred to the respective theoretical density (TD), calculated by the rule of mixture, taking values of 3.96 g/cm^3 [20], 4.55 g/cm^3 (ICDD file no. 33-0040), and 5.82 g/cm^3 (ICDD file no. 77-2112) for fully dense α-alumina, YAG and c-ZrO_2, respectively.

The fired microstructures were submitted to FESEM characterization (Hitachi S4000), performed on polished surfaces. By image analysis (Scandium soft imaging system software) the mean grain sizes of matrix and second phases in the three composites were determined, measuring at least a hundred grains for each phase.

Mechanical characterization

The Vickers micro-hardness was tested on all the samples by applying a maximum load of 300 g_f for 15 s (Wolpert Group, Micro-Vickers Hardness Tester Digital Auto Turret, Mod. 402MVD). For each indentation, the length of the two diagonals was measured and the corresponding hardness was determined according to standard equations [25]. The mean value of the Vickers hardness was calculated using data from at least 10 clearly readable, not cracked or deformed indentations. For comparison, Vickers hardness data were collected on both slip cast and pressed materials.

Moreover, the local elastic properties of the slip cast composites were determined by means of a depth-sensing nano-indentation technique (OpenPlatform, C·S.M. Instruments, equipped with a Berkovitch indenter tip); a maximum load of 500 mN was applied for 15 s and the elastic modulus was calculated from the load-penetration depth curve, automatically recorded by the instrument, according to the Oliver and Pharr approach [26]. The nano-indenter allowed a strict control of the test location and a fine detection of the reached penetration depth (nominal depth resolution: 0.04 nm [27]). At the same time, due to the relatively high load used in the present test, a global response of the material was obtained, reflecting the overall behavior of the composite system and not simply that of the single constituent phases (indicatively, the dimension of the impression was about 8–10 μm). With the aim of obtaining representative values of the elastic properties, at least 20 indentations were performed on each sample.

In order to estimate the fracture toughness, also high-load indentations were carried out on the composites (OpenPlatform, C·S.M. Instruments, equipped with a Vickers indenter tip); the maximum load, set at 30 N, was applied for 15 s. For each impression, the length of the diagonals and that of the cracks were measured by SEM observations and the corresponding value of K_{IC} was determined according to the Evans and Charles equations [28]. For each composite, at least 5 indented scars were evaluated.

Results and discussion

Composite powders elaboration

c-ZrO_2 was yielded in AZ after calcination at 600 °C for 1 h: as reported in Fig. 1a, besides α-Al_2O_3 XRD peaks, $Zr_{0.72}Y_{0.28}O_{1.862}$ phase was detected (ICDD no. 77-2112), proving the effectiveness of yttrium in fully stabilizing cubic ZrO_2. This powder was effectively dispersed in water by ball-milling for 96 h, as shown in Fig. 1b, in which the particle size distributions before (solid line) and after (triangles) dispersion are compared.

As regards AY, YAG crystallization was yielded only after higher-temperature calcination, for instance at 1200 °C for 30 min. The XRD pattern of this sample is presented in Fig. 2a (curve I), showing a quite well crystallized garnet phase (ICDD no. 33-0040), besides monoclinic $Al_2Y_4O_9$ (ICDD no. 34-0368, YAM), and orthorhombic perovskite $YAlO_3$ (ICDD no. 33-0041, YAP). However, such a high-temperature treatment induced the formation of hard agglomerates, poorly dispersed even after 144 h ball-milling (see Fig. 2b). Consequently, the pretreatment temperature was lowered to 1050 °C, and the role of conventional and fast calcination was investigated. In the former case, YAM crystallized (curve II of Fig. 2a), in the latter, YAP phase was identified (curve III). Both these intermediate phases converted to YAG after calcination in the 1300°–1500 °C temperature range, yielding highly-pure composite powders [21, 22]. In any case, fast calcination was preferred, since it allowed to obtain finer crystallites [24]. In addition, the 1050 °C-fast calcined powder showed a good dispersability, since it was effectively de-agglomerated after 48 h of ball-milling (see Fig. 2b).

On the ground of AZ and AY phase evolution, AZY was previously calcined at 600 °C for 1 h (promoting zirconia crystallization) and then submitted to fast heating at 1050 °C for 5 min (to yield crystalline yttrium aluminates). Powder dispersion was then achieved after 96 h of ball-milling.

For the sake of clarity, Table 1 collects the average agglomerate sizes of AZ, AY, and AZY calcined and ball-milled powders, showing comparable values in all materials.

Forming, sintering and microstructural characterization

The green densities of the slip cast and uniaxially pressed bodies are collected in Table 2, showing slightly higher values for the former samples. It suggests a more effective particle packing in the green compacts produced by the wet-forming method [29]. The sintered density of all composites is collected in Table 2, as well. Full densification was reached by all slip cast samples, whereas slightly lower values were determined for the pressed ones. Such differences can be easily explained by comparing the microstructure of the slip cast and pressed samples. For instance, in Fig. 3, the microstructures of AZY pressed (a) and slip cast (b) materials are shown. The former presents a dense microstructure, made of quite regular-shaped grains, but some large defects, probably created during the cold uniaxial pressing of oven-dried powders, led to a lowering of the final density. In contrast (Fig. 3b), an almost defect-free sample, in which both second phases are homogeneously distributed into the alumina matrix, was produced by slip casting.

Figure 4 compares, indeed, the microstructures of slip cast AZY (a), AY (b), and AZ (c) samples. Fully dense

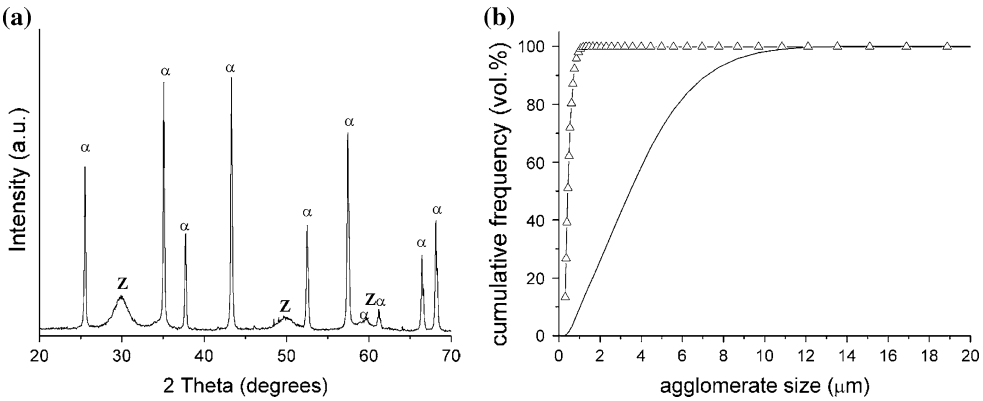

Fig. 1 **a** XRD patterns of AZ calcined at 600 °C for 1 h (α = α-Al_2O_3; Z = cubic ZrO_2); **b** particle size distribution of the same powder before (*solid line*) and after (*triangles*) dispersion

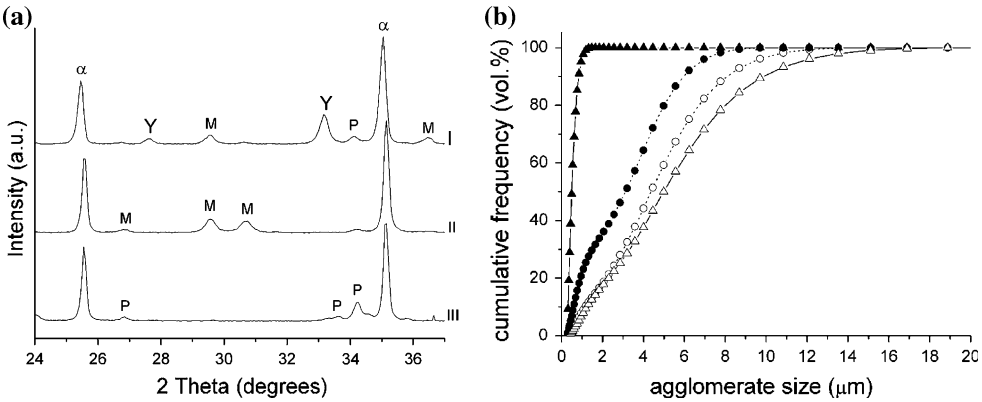

Fig. 2 **a** XRD patterns of AY calcined at 1200 °C for 30 min (*I*) and at 1050 °C for 5 min by conventional (*II*) and fast (*III*) treatments ($\alpha = \alpha$-Al_2O_3; *Y* YAG; *M* YAM; *P* YAP); **b** particle size distribution of AY conventionally calcined at 1200 °C for 30 min (*circles*) and fast heated at 1050 °C for 5 min (*triangles*), before (*empty symbols*) and after (*full symbols*) dispersion

Table 1 d_{10}, d_{50} and d_{90} values for calcined and ball-milled AZ, AY and AZY powders

Sample	d_{10} (μm)	d_{50} (μm)	d_{90} (μm)
AZ	0.28	0.46	0.77
AY	0.33	0.52	0.87
AZY	0.30	0.48	0.83

microstructures were observed in all materials, and the second phases were always very well distributed, also in the case of AZY (the slightly different phase contrast between the two reinforcing phases allow to distinguish them, with zirconia being the brightest one). However, a systematic observation supported by image analysis allowed to point out some microstructural differences among the three composites. For the sake of clarity, Table 3 collects the average alumina, YAG and c-ZrO_2 grain size in AZ, AY and AZY.

The average alumina grain size in AZY is slightly lower as compared with the respective biphasic materials. In addition, it presents a significantly smaller standard deviation than the AZ and AY ones, denoting a narrower grain size distribution of the alumina matrix inside the three-phase composite. Also the zirconia grains were finer in AZY as compared with AZ material; in fact, the higher zirconia amount in the biphasic composite gave rise to a more relevant grain growth as compared with the triphasic one, where the c-ZrO_2 concentration was reduced by half. As far as the YAG phase is concerned, almost the same mean grain size was determined in AZY and AY; however, in the latter sample, coalescence of YAG sometimes occurred, giving rise to second phase *clusters* inside the composite (see the insert of Fig. 4b). This feature was indeed rarely observed in the triphasic material. The better YAG phase distribution and the finer zirconia grain size in AZY, in comparison with the respective biphasic composites, can justify its finer matrix grain size.

Table 2 Green density, fired density and Vickers micro-hardness for slip cast and pressed AZ, AY and AZY samples (The error (±) indicates the standard deviation)

Sample	Forming method	Green density (g/cm^3)	Fired density (% of TD)	HV (HV0.3)
AZ	Slip casting	2.35	99.1	1947 ± 141
AZ	Pressing	2.15	98.8	1700 ± 134
AY	Slip casting	2.58	99.9	1989 ± 129
AY	Pressing	2.36	98.3	1660 ± 127
AZY	Slip casting	2.38	99.5	1936 ± 144
AZY	Pressing	2.27	98.9	1548 ± 153

Mechanical characterization

The results of the Vickers micro-indentation tests performed on both slip cast and pressed samples are reported in Table 2. The obtained values suggest that a strong dependence of the Vickers hardness on the manufacturing technique exists, since the samples obtained via slip casting were harder than the respective ones produced via pressing, as expected from the slightly higher density of the former materials.

If the hardness of the three slip cast samples is compared, similar and very high values can be observed, since all samples present hardness ranging between 19 and 19.5 GPa. To explain the slightly different values, the three main parameters able to affect hardness, i.e. sintered density, grain size, and hardness of the constituent phases, have to be considered.

Literature offers a variety of HV values for corundum; however, values of about 15.5–16.5 GPa were given for sintered alumina with grain size ranging between 1 and 5 μm [30], whereas higher values of about 18–19 GPa were found for a submicron-sized material [31]. c-ZrO_2 presents HV values in the range 12.6–12.8 GPa [32, 33], whereas slightly lower values of 12–12.5 GPa are given for YAG [34, 35]. On the basis of these data, a lower hardness was expected for AY whose HV was, on the contrary, the

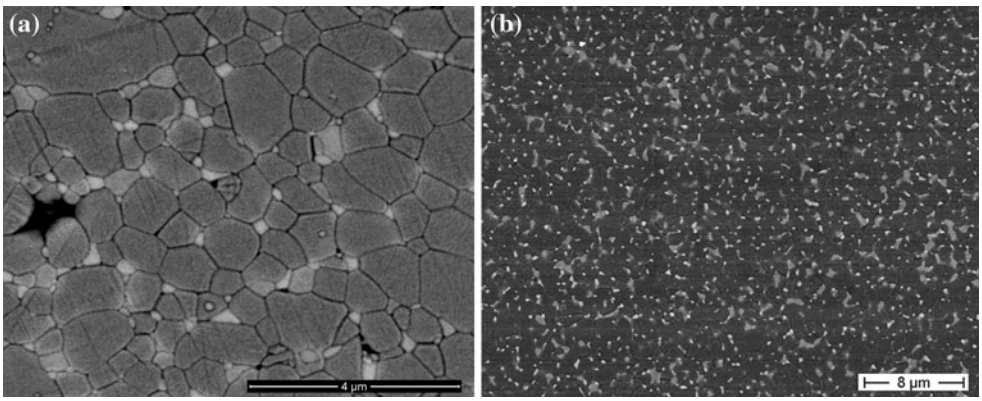

Fig. 3 FESEM micrographs of pressed (**a**) and slip cast (**b**) AZY

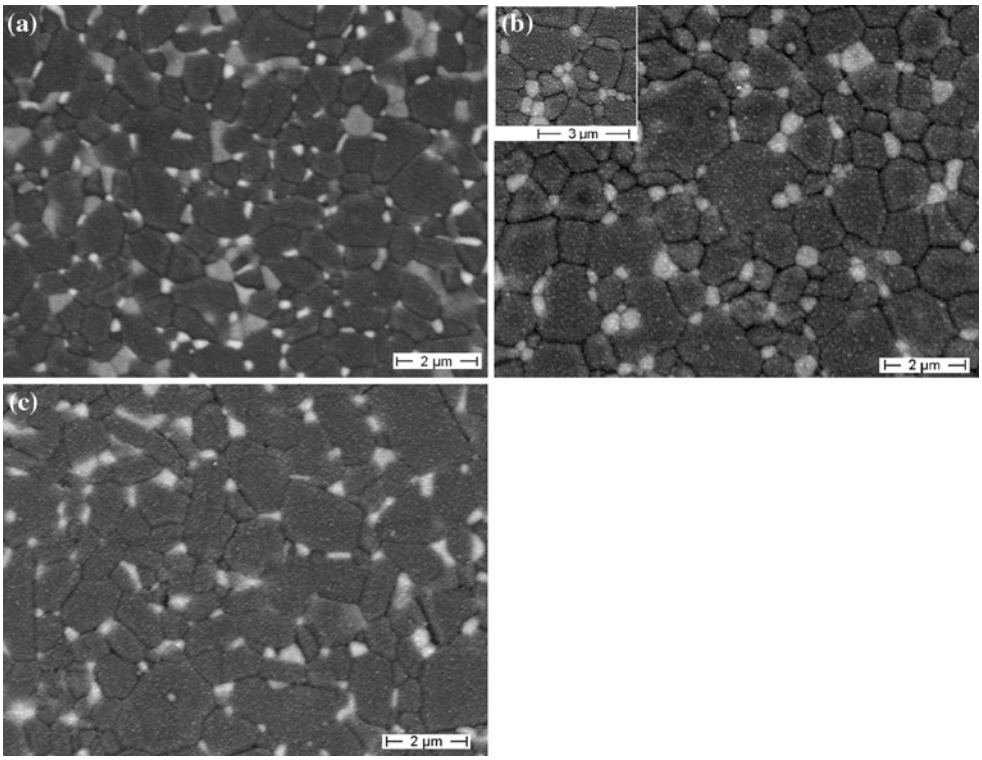

Fig. 4 FESEM micrographs of slip cast AZY (**a**), AY (**b**) and AZ (**c**)

Table 3 Average grain size of Alumina, YAG and ZrO_2 in slip cast AZ, AY and AZY composites (The error (±) indicates the standard deviation)

Sample	Al_2O_3 (μm)	YAG (μm)	FSZ (μm)
AZ	1.16 ± 0.48	–	0.45 ± 0.14
AY	1.09 ± 0.41	0.44 ± 0.12	–
AZY	0.91 ± 0.29	0.48 ± 0.15	0.31 ± 0.08

highest one. So, in our case, the sintered density seemed to play the major role, AY being the denser material. This feature seems to predominate over the composite grain size: in fact, a slightly lower HV value was found for AZY in spite of its finer microstructure.

Few hardness data are reported in the literature for the investigated systems; however, values in the range 16–19.5 GPa were found for composites made by a micronic alumina matrix and fine YAG particles contained between 10 and 25 vol.% [4, 30]. In addition, values in the range 16–19 GPa were found for an Alumina–Yttria–Zirconia particulate composite [19], having eutectic composition. The obtained values were, on average, higher than those usually observed for sintered α-alumina [36]; such increment could be due to the concomitant effects of the

Table 4 Experimental elastic modulus (E_{exp}), ROM-calculated elastic modulus (E_{ROM}) and fracture toughness (K_{IC}) of slip cast AZ, AY and AZY samples (for experimental data, E_{exp} and K_{IC}, the error (±) indicates the standard deviation)

Sample	E_{exp} (GPa)	E_{ROM} (GPa)	K_{IC} (MPa $m^{1/2}$)
AZ	323 ± 19	390	3.5 ± 0.2
AY	351 ± 28	397	3.7 ± 0.2
AZY	331 ± 33	394	3.6 ± 0.2

dispersed phases (YAG and/or zirconia) and, most of all, of the very fine nature of the microstructure.

Table 4 reports the elastic modulus and fracture toughness of the slip cast samples. As already observed for the Vickers hardness, also in this case, comparable values were found for the three composites. Once again, this may suggest that the sintered density plays the key role in assuring high mechanical properties.

As a general trend, the Young's modulus of the three composite systems was lower than that of pure α-alumina: Munro, for example, attested a Young's modulus of about 416 GPa for a sintered α-alumina, with a nominal grain size of 5 μm [36]. According to the temperature-dependent equations proposed by Ochiai et al. [37], a modulus of about 409 GPa may be assumed at room temperature (298 K) [37]. However heterogeneous values for the Young's modulus of alumina and alumina-matrix composites can be found in the literature, due to the different measurement methods employed. In fact, several articles in the literature report the results of resonance-based tests, while other contributions (including the present one) rely on nano-indentation, which could be particularly sensitive to local effects [38]. Most of all, it should be considered that YAG [37, 39] and c-ZrO_2 [40, 41] phases are characterized by values of the Young's modulus much lower than that usually declared for alumina. So, the introduction of such phases is expected to induce a decrement of the mean elastic properties of the composites with respect to pure alumina. A rough estimate of the effect of the second phases on the Young's modulus can be provided by the rule of mixture (ROM) [42], assuming for the calculation $E_{Al_2O_3} = 409$ GPa (according to Ochiai et al. [37]), $E_{YAG} = 294$ GPa [37] and $E_{c-ZrO_2} = 221$ GPa [40]. The results are reported in the same Table 4. The ROM-derived moduli generally overestimate the experimental values, since the ROM is an upper bound [42]. However the trend is the same, being the Young's modulus progressively lower in the series AZ-AZY-AY. This suggests that the Young's modulus of the composite material is particularly sensitive to the addition of c-ZrO_2, whose Young's modulus is lower than that of YAG.

Not only the elastic modulus, but also the fracture toughness of the tri-phase composite is comparable with that of the bi-phase systems and the obtained value fits well with those published by Oelgardt et al. for composites having eutectic composition [19]. The detailed observation of a representative crack propagating from an indent in the triphasic composite is shown in Fig. 5, obtained by connecting several FESEM micrographs. In the near-indent region, the propagation is mainly trans-granular (double arrows in Fig. 5), due to the high energy associated to the newly formed crack and the local stress concentration caused by the sharp vertex of the impression. Apart from this initiation area, the crack becomes mainly trans-granular in the pure alumina regions (white arrows), especially if the alumina grains are relatively large. This suggests the very strong adhesion existing at the alumina grain boundaries. Instead, if grains of a second phase are present, the crack runs preferentially at the grain boundary (black arrows) and this process is particularly evident in the presence of c-ZrO_2 grains. In fact the change from a trans-granular propagation to an inter-granular one may be favored by the development of thermal residual stresses at the interface between the alumina grains and the second phase ones. Generally speaking, in ceramic composites the particles are expected to be in a state of strong mechanical stress as a consequence of the different coefficients of thermal expansion of the constituent phases [43]. The hydrostatic stress P acting on the particles can be predicted by means of the Selsing Eq. 1 [43, 44]:

$$P = \frac{\Delta\alpha \cdot \Delta T}{\frac{1+\nu_m}{2E_m} + \frac{1-2\nu_p}{E_p}}, \quad \Delta\alpha = \alpha_p - \alpha_m \tag{1}$$

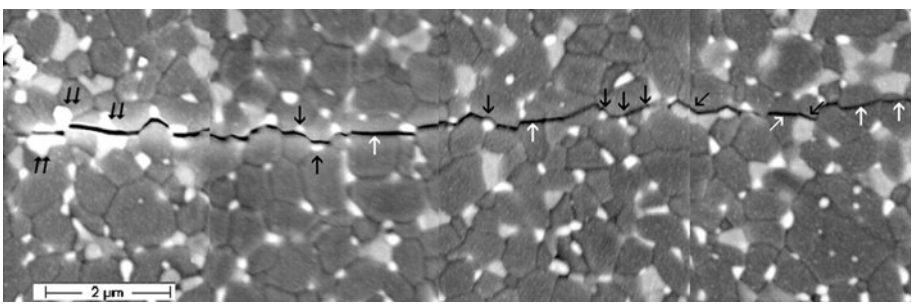

Fig. 5 Connected FESEM micrographs showing a representative, whole crack propagation in AZY material

where the subscripts m and p refer to the matrix and particle, respectively; E, ν, and α are the Young's modulus, the Poisson's coefficient and the coefficient of thermal expansion; ΔT is the difference between the temperature at which the matrix stops to flow on cooling and room temperature [43]. For composite systems having a glassy matrix, the temperature at which the matrix ceases to flow may be assimilated to the glass transition temperature; in the present case, as suggested by Ochiai et al. [37], it was associated to the temperature at which the dislocation movement in the alumina matrix stops and hence it was set to 1423 K [37], so that $\Delta T = (1423 - 298\ \text{K}) = 1125$ K. For calculation, the same previously reported elastic molduli were used, whereas the Poisson's coefficients were: $\nu_{Al_2O_3} = 0.23$ [37], $\nu_{YAG} = 0.25$ [37], and $\nu_{c-ZrO_2} = 0.32$ [40]. Finally, the coefficients of thermal expansions were considered to be: $\alpha_{Al_2O_3} = 6.94 \times 10^{-6}\ \text{K}^{-1}$ [37], $\alpha_{YAG} = 6.44 \times 10^{-6}\ \text{K}^{-1}$ [37], and $\alpha_{c-ZrO_2} = 10.0 \times 10^{-6}\ \text{K}^{-1}$ [45]. By substituting these values into Eq. 1, the calculated P was 1.09 GPa (tensile) for c-ZrO_2 inclusions and −0.17 GPa (compressive) for YAG particles. These results are affected by two limitations: first of all, the dependence of the thermo-elastic properties (E, ν, and α) on the temperature was not considered, even if the $\Delta T = 1125$ K was significant; the Selsing Eq. 1 applies to biphasic systems only, so it was used to calculate separately the stresses at alumina–zirconia and alumina-YAG interfaces, thus neglecting the zirconia-YAG interfaces and the triple junctions (which, however, are statistically rare). Nevertheless the Selsing equation makes it possible to appreciate the development of significant thermal residual stresses at the interface between the alumina matrix and the reinforcements, which is likely to interfere with the crack propagation favoring the observed inter-granular paths.

Conclusions

The described elaboration route was successful in producing high purity composites, having bi- and tri-phase compositions. Precisely, Al_2O_3–10 vol.%YAG (AY), Al_2O_3–10 vol.%ZrO_2 (AZ), and Al_2O_3–5 vol.%YAG-5 vol.% ZrO_2 (AZY) composites were developed.

Green bodies, produced by both uniaxial pressing or slip casting, were pressureless sintered at 1500 °C for 3 h. Slip casting gave rise to denser green bodies (due to a better particles packing) and to defect-free sintered materials, characterized by a highly homogeneous distribution of the second phases in all compositions. If the mean grain sizes of the matrix and second phases in the bi- and tri-phase systems are compared, a slightly finer microstructure was found in AZY, due to a finer zirconia grain size and to a better YAG distribution as compared with the respective bi-phasic materials.

On account of its dense and fine microstructure, the new tri-phase composite could reach high values of Vickers hardness (HV = 19.0 ± 1.4 GPa), elastic modulus (E = 331 ± 33 GPa), and fracture toughness ($K_{IC} = 3.6 \pm 0.2$ MPa $m^{1/2}$). The mechanical characterization of the three slip cast samples proved that the Vickers hardness mainly relied on the sintered density, while the elastic modulus depended on the volume fractions of the constituent phases, as predicted by the rule of mixture. The fracture toughness and, most of all, the crack propagation paths were deeply influenced by the development of thermal residual stresses at the alumina matrix-second phase particles interface.

Acknowledgements Eng. Andrea Cattini is kindly acknowledged for his contribution in the experimental activity.

References

1. Sternitzke M (1997) J Eur Ceram Soc 17:1061
2. Towata A, Hwang HJ, Yasuoka M, Sando M, Niihara K (1998) J Am Ceram Soc 81:2469
3. Wang H, Gao L (2001) Ceram Int 27:721
4. Li W, Gao L (1999) Nanostruct Mater 11:1073
5. Duong H, Wolfestine J (1993) Mater Sci Eng A 172:173
6. French JD, Zhao J, Harmer MP, Chan HM, Miller GA (1994) J Am Ceram Soc 77:2857
7. Torrecillas R, Schehl M, Diaz LA, Menendez JL, Moya JS (2007) J Eur Ceram Soc 27:143
8. Parthasarathy AP, Mah TI, Keller K (1992) J Am Ceram Soc 75:1756
9. Chevalier J, Grandjean S, Kuntz M, Pezzotti G (2009) Biomaterials 30:5279
10. Sadangi RK, Shukla V, Kear BH (2005) Int J Refract Met Hard Mater 23:363
11. Guimaraes FAT, Silva KL, Trombini V, Pierri JJ, Rodrigues JA, Tomasi R, Pallone EMJA (2009) Ceram Int 35:741
12. Tuan WH, Chen RZ, Wang TC, Cheng CH, Kuo PS (2002) J Eur Ceram Soc 22:22827
13. Hannink RHJ, Kelly PM, Muddle BC (2000) J Am Ceram Soc 83:461
14. Chen T, Tekeli S, Dillon RP, Mecartney ML (2008) Ceram Int 34:365
15. Taherabadi L, Trujillo JE, Chen T, Porter JR, Mecartney ML (2008) J Eur Ceram Soc 28:371
16. Schehl M, Torrecillas R (2002) Acta Mater 50:1125
17. Torrecillas R, Schehl M, Diaz LA (2007) J Eur Ceram Soc 27:4613
18. Kim DK, Kriven WM (2008) J Am Ceram Soc 91:793
19. Oelgardt C, Anderson J, Heinrich JG, Messing GL (2010) J Eur Ceram Soc 30:649
20. http://www.taimei-chem.co.jp
21. Palmero P, Naglieri V, Chevalier J, Fantozzi G, Montanaro L (2009) J Eur Ceram Soc 29:59
22. Naglieri V, Palmero P, Montanaro L (2009) J Therm Anal Calorim 97:231
23. Naglieri V, Joly-Pottuz L, Chevalier J, Lombardi M, Montanaro L (2010) J Eur Ceram Soc 30:3377

24. Palmero P, Naglieri V, Spina G, Lombardi M (2011) Ceram Int 37:139
25. Quinn GD, Patel PJ, Lloyd I (2002) J Res Natl Inst Stan 107:299
26. Oliver WC, Pharr GM (1992) J Mater Res 7:1564
27. CSM indentation testers catalogue. http://www.csm-instruments.com/it/webfm_send/51. Accessed on 1 Jun 2010
28. Ponton CB, Rawlings RD (1989) Mater Sci Tech 5:865
29. Azar M, Palmero P, Lombardi M, Garnier V, Montanaro L, Fantozzi G, Chevalier J (2008) J Eur Ceram Soc 28:1121
30. Lach R, Haberko K, Bucko MM, Szumera M, Grabowski G (2011) J Eur Ceram Soc 31:1889
31. Krell A, Schädlich S (2001) Mater Sci Eng A307:172
32. De Aza AH, Chevalier J, Fantozzi G, Schehl M, Torrecillas R (2002) Biomaterials 23:937
33. Tekeli S (2006) Mater Design 27:230
34. Ikesue A, Furusato I (1995) J Am Ceram Soc 78:225
35. Li J, Wu YS, Pan YB, Liu B, Huang LP, Guo JK (2008) Opt Mater 31:6
36. Munro RG (1997) J Am Ceram Soc 80:1919
37. Ochiai S, Ikeda S, Iwamoto S, Sha JJ, Okuda HH, Waku Y, Nakagawa N, Mitani A, Sato M, Ishikawa T (2008) J Eur Ceram Soc 28:2309
38. VanLandingham MR (2003) J Res Natl Inst Stan 108:249
39. Yagi H, Yanagitani T, Numazawa T, Ueda K (2007) Ceram Int 33:711
40. Selçuk A, Atkinson A (1997) J Eur Ceram Soc 17:1523
41. NIST Property Data Summaries—Elastic moduli data for polycrystalline ceramics. http://www.ceramics.nist.gov/srd/summary/ZrO2cY.htm. Accessed 1 Jun 2010
42. Gibson RF (1994) Principles of composite material mechanics. McGrow-Hill International Editions, New York
43. Zwanziger JW, Werner-Zwanziger U, Zanotto ED, Rotari E, Glebova LN, Glebov LB, Schneider JF (2006) J Appl Phis 99:083511
44. Selsing J (1961) J Am Ceram Soc 44:419
45. Mori M, Abe T, Itoh H, Yamamoto O, Takeda Y, Kawahara T (1994) Solid State Ionics 74:157